

# Protective radiolucent aluminium oxide coatings for beryllium X-ray optics

Oksana Yurkevich,<sup>a\*</sup> Ksenia Maksimova,<sup>a</sup> Alexander Goikhman,<sup>a</sup> Alexey Grunin,<sup>a</sup> Pavel Prokopovich,<sup>a</sup> Alexander Tyurin,<sup>b</sup> Polina Medvedskaya,<sup>c</sup> Ivan Lyatun,<sup>c</sup> Irina Snigireva<sup>d</sup> and Anatoly Snigirev<sup>c</sup>

Received 19 December 2016

Accepted 29 May 2017

Edited by A. Momose, Tohoku University, Japan

**Keywords:** beryllium optics;  
protective coatings; aluminium oxide.

<sup>a</sup>Research and Educational Centre 'Functional Nanomaterials', Immanuel Kant Baltic Federal University, Nevskogo Street 14, Kaliningrad 236041, Russian Federation, <sup>b</sup>Research and Educational Center 'Nanotechnologies and Nanomaterials', G. R. Derzhavin Tambov State University, Zashitniy Pereulok 7, Tambov 392000, Russian Federation, <sup>c</sup>X-ray Optics Laboratory, Immanuel Kant Baltic Federal University, Nevskogo Street 14, Kaliningrad 236041, Russian Federation, and <sup>d</sup>European Synchrotron Radiation Facility, 6 rue Jules Horowitz, 38043 Grenoble, France.

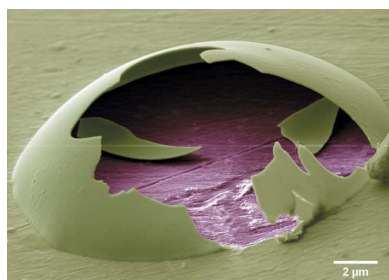
\*Correspondence e-mail: oyurkevich@innopark.kantiana.ru

Beryllium, being one of the most transparent materials to X-ray radiation, has become the material of choice for X-ray optics instrumentation at synchrotron radiation sources and free-electron laser facilities. However, there are concerns due to its high toxicity and, consequently, there is a need for special safety regulations. The authors propose to apply protective coatings in order to seal off beryllium from the ambient atmosphere, thus preventing degradation processes providing additional protection for users and prolonging the service time of the optical elements. This paper presents durability test results for Be windows coated with atomic-layer-deposition alumina layers run at the European Synchrotron Radiation Facility. Expositions were performed under monochromatic, pink and white beams, establishing conditions that the samples could tolerate without radiation damage. X-ray treatment was implemented in various environments, *i.e.* vacuum, helium, nitrogen, argon and dry air at different pressures. Post-process analysis revealed their efficiency for monochromatic and pink beams.

## 1. Introduction

Beryllium has the lowest X-ray absorption coefficient of any solid state material available under normal conditions and at the same time has a relatively high refractive index. These properties make Be particularly favourable for the manufacturing of windows and compound refractive lenses (Snigirev *et al.*, 1996) for synchrotron radiation facilities and X-ray free-electron lasers (Winick & Doniach, 1980). However, there is a significant drawback in utilizing Be optics due to material oxidation and subsequent degradation under powerful X-ray irradiation (Gmür, 1992). Beryllium possesses a grain structure; contamination and moisture condensation on the grain boundaries as well as contact of the grain boundary with a metal support can break the integrity of the vacuum-tight window. There are serious health risks associated with powder BeO which can be formed under powerful X-ray irradiation (Gmur, 1988). Beryllium oxide in its powder state is toxic for humans when inhaled. Improved properties of X-ray optics in terms of their surface quality and higher stability in the powerful X-ray beams are required as the high-brilliant fourth generation of synchrotrons are now being developed (Tanaka *et al.*, 2016).

Nowadays, the majority of synchrotrons have mandatory technical regulations that require blowing Be elements with



inert gas or using them under vacuum conditions so as not to expose them to ambient atmosphere, thus preventing the destructive oxidation processes of Be optical elements and meeting safety requirements. This often results in increasing complexity of experimental equipment and optical schemes.

We propose to apply passivation coatings on the X-ray optical elements for protecting the beryllium elements and the researchers working with them (Yurkevich *et al.*, 2015). Aluminium oxide is a well known passivation material (Fedel *et al.*, 2014; Härkönen *et al.*, 2011) which is hard, chemically inert and has good thermal properties. The low-Z number of Al<sub>2</sub>O<sub>3</sub> compounds provides for its relatively low X-ray absorption coefficient ([http://henke.lbl.gov/optical\\_constants/](http://henke.lbl.gov/optical_constants/)), whereas usage of a thin film with a thickness of only a few dozens of nanometers helps to preserve the radiolucency of the Be optical elements. The following requirements were used to select a deposition technique: good adhesion of the thin film toward the substrate, a pinhole-free coating and conformal deposition of objects with complicated configuration, such as the high-aspect-ratio parabolic shape of compound refractive lenses. To meet these requirements we opted for the atomic layer deposition (ALD) technique (Knez *et al.*, 2007). Chemisorption reactions in the ALD technique provide perfect adhesion (Ylivaara *et al.*, 2014) by forming chemical bonds between the deposited material and the substrate. The cyclic manner of precursors delivery makes it possible to deposit conformal ultra-thin coatings on high-aspect-ratio objects and control their thickness precisely (Elam *et al.*, 2003). All the above-mentioned advantages make ALD a key enabling technique for depositing on X-ray windows, lenses and zone plates with complex surface profiles.

In the present study, the durability of Al<sub>2</sub>O<sub>3</sub> thin films deposited by the ALD method on beryllium substrates was tested under monochromatic-, pink- and white-beam irradiation at various compositions and pressures of the gas medium to simulate the real work regimes during synchrotron experiments. This study focuses on the investigation of samples exposed under the white beam as it is the most extreme condition for the coating to withstand. Chemical properties of the coatings were checked before and after the white-beam exposition by Auger electron spectroscopy (AES). Post-process visualization by optical and scanning electron microscopies (SEM) was performed. The mechanical properties of the protective layers were established.

**Table 1**  
Samples exposed to white beam at station ID06 for different conditions.

Gaseous medium	Pressure	Exposition time (h)	Estimated Al <sub>2</sub> O <sub>3</sub> thickness (nm)
Vacuum	10 <sup>-6</sup> mbar	2; 9	35
Vacuum	10 <sup>-6</sup> mbar	2; 9	70
Air	1.3 mbar	2; 9	35
Air	1.1 bar	2; 9	70
He	1.3 mbar	2; 9	70
He	1.1 bar	2; 9	70
N <sub>2</sub>	1.1 bar	2; 9	70
Ar	1.3 mbar	2; 9	70

## 2. Experiment

Polished beryllium substrates (Materion, high purity, vacuum-tight PF-60 and IF-1 grades) were covered with thermal ALD alumina. Deposition was carried out in a commercially available SVTA reactor with trimethylaluminium and water precursors. Continuity of the deposited layers was checked *in vacuo* by surface-sensitive secondary mass ion spectroscopy. X-ray diffraction measurements proved the amorphous structure of the alumina oxide coating. The thickness of alumina and its stoichiometry were studied by Rutherford backscattering spectroscopy (RBS) using He ions of energy 1.7 MeV. The RBS data proved the desired stoichiometry of the elements, Al:O = 2:3, and the absence of heavy impurities which is crucial for durability under the X-rays. Since beryllium material has a grain structure, and every Be grain is surrounded by beryllium oxide (Lyatun *et al.*, 2015; Goikhman *et al.*, 2015), a small incorporation of oxygen in the Be substrate was detected.

Stability tests of the formed coatings were carried out at the ESRF, Grenoble, France. Exposition of the samples under white-beam undulator u18u irradiation at ID06 (the so-called ‘white-beam test’) was performed in different gaseous environments. Undulator u18u is a cryogenic permanent-magnet undulator with a period of 18 mm, minimum gap of 6.05 mm at 200 mA and maximum gap of 30.00 mm. Samples were fixed at a special holder with a small contact area to reduce heat exchange and placed inside the chamber as shown in Fig. 1. The possibility of using vacuum or constant inert gas flow allows irradiation tests in argon, helium, dry air, nitrogen and vacuum atmospheres to be performed. Besides, the irradiation time and pressure inside the chamber varied. Each sample was irradiated for both 2 and 9 h, as listed in Table 1. The white-

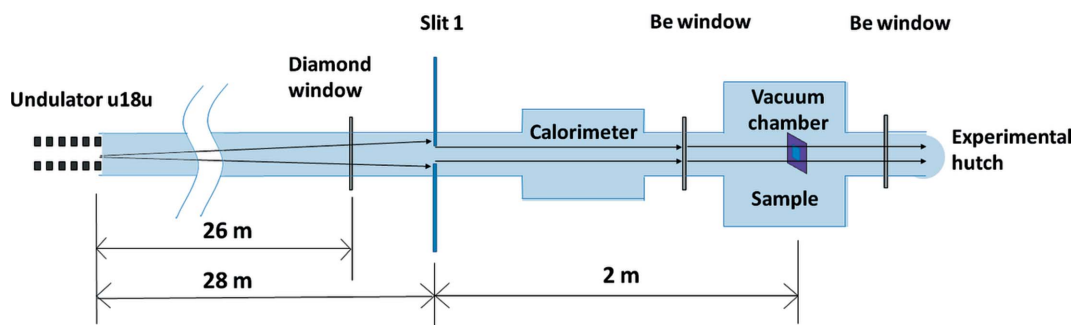


**Figure 1**  
Experimental scheme of the white-beam test at ID06.

beam energy range was from 5 keV up to 100 keV,  $\sim 200$  mA current, and the total heat-load power flux applied to the samples was  $640 \text{ W mm}^{-2}$  at 6.75 mm gap, as measured by calorimeter.

Exposition of the samples under the 12 keV monochromatic beam at beamline ID06 took 24 h under the ambient atmosphere. Irradiation under the pink beam at 7 keV and  $\Delta E = 600 \text{ eV}$  was performed at beamline ID24 for about a month-long period with periodic abruptions of the exposition. The sample was installed as a window separating the vacuum chamber and ambient atmosphere.

The chemical composition of the exposed areas was studied by RBS and AES measurements. After irradiation of some samples, surface degradation was detected which led to the so-called blistering development. Visualization and investigation of blistering was carried out by SEM in backscattered and secondary electron regimes.

To study the local physico-mechanical properties, we applied a TI-950 Triboindenter (Hysitron, USA) nano-indenter, which allows the nanohardness ( $H$ ) and Young's modulus ( $E$ ) to be determined in a thickness range from several nanometers to a few micrometers. Determination of  $H$  and  $E$  was based on the Oliver–Pharr method (Oliver & Pharr, 2004), which consists of continuous measurement of applied force  $P$  and indentation depth  $h$  and plotting of  $P(h)$  diagrams taking into account the real geometry of the indenter. A Berkovich indenter was used for indentation.

### 3. Results and discussion

After exposing the samples under the white beam, changes in the topography of the irradiated areas were visible to the naked eye. Optical microscopy was performed first to check surface modifications (Fig. 2). The modifications observed are called blistering or buckling; they strongly depend on the exposition conditions (Table 1). Different density and size distributions of the blisters occurred. In the case of a small density, the distribution of blisters was not homogeneous. They mainly appeared in the irradiated region but a few of them were found at a small distance outside this area.

For further study of the surface topography, visualization of the blisters was made by SEM measurements; typical images are shown in Figs. 3(a) and 3(b). Features which have been

observed are usually associated with a local delamination of a thin film under excessive compressive stress. In recent works the origin of the buckling is linked with the overheating of the alumina thin films prepared by the ALD method (Beldarrain *et al.*, 2013). It was proved that the driving force for the buckling is hydrogen conglomeration on the substrate/film interface, so blistering is not only caused by residual stress. Hydrogen contamination in the film is a result of the precursor choice; both  $\text{Al}(\text{CH}_3)_3$  and  $\text{H}_2\text{O}$  contain hydrogen atoms. As the main growth mechanism for ALD is ligand exchange, some of the ligands can remain unreacted, mainly due to steric factors. Therefore, hydrogen and water contaminants are found in the film volume as well as on the substrate interface. During the film annealing at temperatures higher than  $400^\circ\text{C}$  (Bullock *et al.*, 2013), hydrogen and water impurities overcome the energy barrier and are released from the bonds with the film, diffusing in both lateral and vertical dimensions

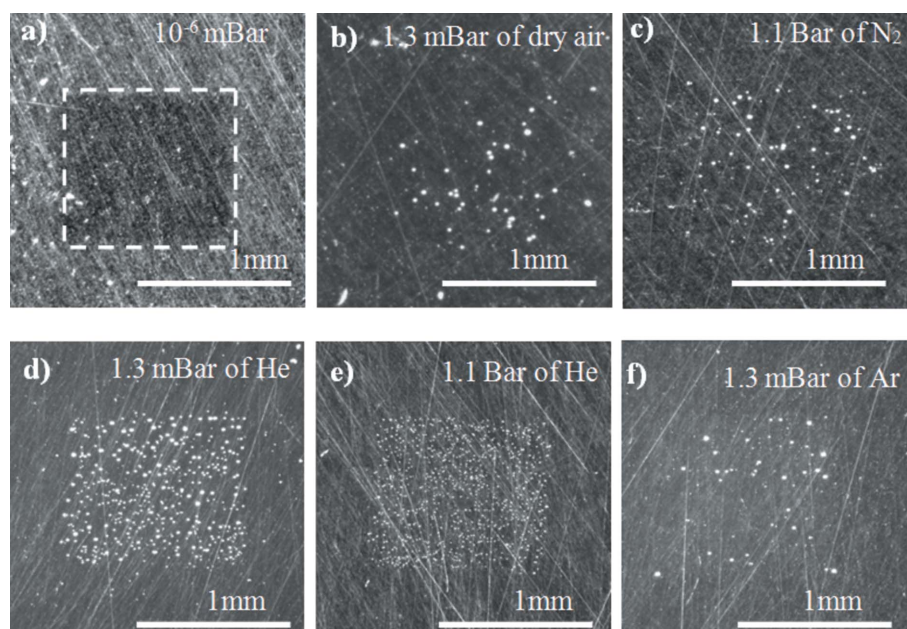


**Figure 2**  
Optical images of the sample irradiated areas after 9 h exposition. The exposed area is marked by the dashed line in (a).

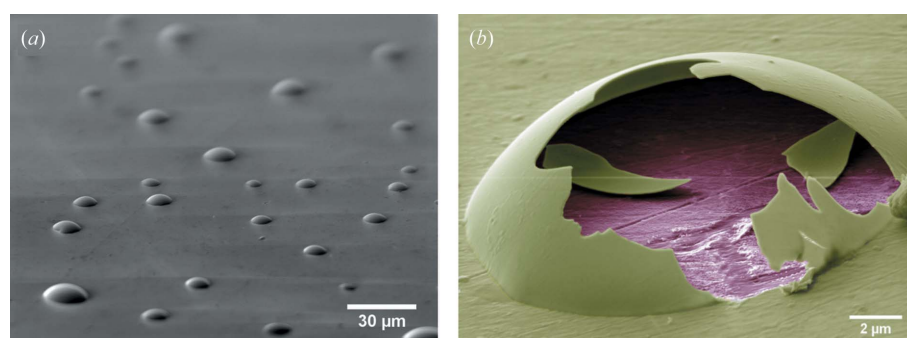


**Figure 3**  
SEM images of blisters on the sample surface after a 9 h white-beam test in (a) He atmosphere at 1.3 mbar pressure and (b) Ar atmosphere at 1.3 mbar pressure. The magenta color corresponds to beryllium and the green color corresponds to alumina.

(Hennen *et al.*, 2012). The blister shown in Fig. 3(b) was broken in vacuum by a micromanipulator to check its inner structure. Using an Auger wide scan, we proved that delamination occurred at the substrate/thin-film interface as there was an uncovered beryllium surface under the blister. This also means that adhesion between layers of thin films is stronger than that of the thin film to the substrate.

In order to trace chemical changes in the irradiated area, a further AES analysis was performed. In the SEM image (Fig. 4b), a clearly visible sharp interface between the exposed (right part) and unexposed (left part) regions

is seen by secondary electrons. Compositional maps from the same area for carbon, beryllium, aluminium and oxygen elements were acquired by AES and are shown in Fig. 4(a). The absence of beryllium on the surface map proved that there was no film abruption. The increase in the carbon level at the irradiated area indicates the formation of carbon deposits under X-ray white-beam irradiation. As a consequence, the signal coming from aluminium and oxygen decreased as the AES analysis depth was approximately 3–5 nm.

Alternating stripes of maximum and minimum intensity of the Auger signal are clearly seen within the elemental map, especially for carbon. These are the Fresnel diffraction pattern fringes of a single straight edge from slit #1 (Fig. 1). The theoretically calculated magnification of the X-ray beam intensity in the first diffraction maximum with a factor of 1.4 (Hecht, 2002) is not reproduced in the elemental map contrast which is enhanced by a 1.07 coefficient only, since we used the beam with a wide wavelength distribution. Except for the first bright edge wave, there are few local intensity maximums that are obtained by the interference between the edge wave and the transmitted wave.

The character of blister formation strongly depends on the irradiation conditions. Blisters occurred mostly in X-ray exposed areas; the distribution of the blister density was estimated utilizing SEM, and is shown in the histogram in Fig. 5.

It can be clearly seen that the blister density depends on the irradiation time. Apparently, radiation damage increases with exposition time. Coating thickness also plays a role: the thinner the film, the less delamination occurred. This can be explained by an increase in the total amount of hydrogen and water impurities, gained with the growth of the film thickness. Therefore, hydrogen-free materials should be used to prevent blister development. For example, ALD Al<sub>2</sub>O<sub>3</sub> can be grown by using AlCl<sub>3</sub> as a metal source (Yun *et al.*, 1997) and O<sub>2</sub> plasma as an oxygen source (Aarik *et al.*, 2014). Accurate disposal of hydrogen and water from the surface interface is also important for the growth of hydrogen-free film.

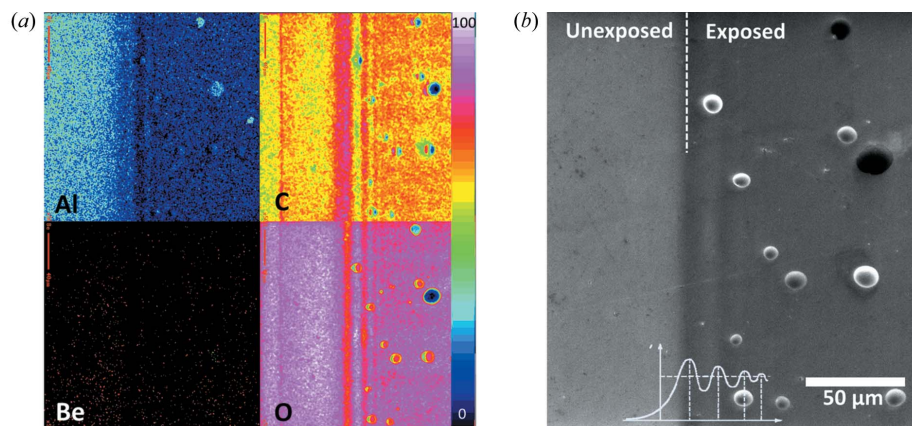


**Figure 4**  
(a) Auger map of the surface elemental composition of the sample with 70 nm thickness of Al<sub>2</sub>O<sub>3</sub> after 9 h irradiation in He atmosphere at 1.3 mbar pressure. The same region is represented *via* SEM (b). Both exposed and unexposed regions were observed (marked on the SEM image).

The strongest impact on blister evolution was induced by the gas atmosphere. The most aggressive environment appeared to be helium. The density of blisters after the white-beam test with 1.1 bar He exceeded 500 blisters per mm<sup>2</sup>, while the density was less than 60 blisters per mm<sup>2</sup> for the white-beam test under vacuum. It is worth noting that with the increase of blister density the size of the blisters reduced. For example, the typical diameter was about 4–6 μm in He atmosphere and 15 μm in N<sub>2</sub>, whereas for an Ar atmosphere this value reached 20 μm [Figs. 2(f) and 3(b)]. It has been reported (Hennen *et al.*, 2012) that there is a trend of an inverse relation between the density and the size of the blisters, so at higher annealing temperatures a higher density of small blisters was observed.

A lower blister density was expected to occur in an atmosphere of air rather than in a vacuum, as air better conducts heat load from the sample and also reduces the intensity of the X-ray beam. However, the white-beam test showed the opposite correlation. This indicates that there was another

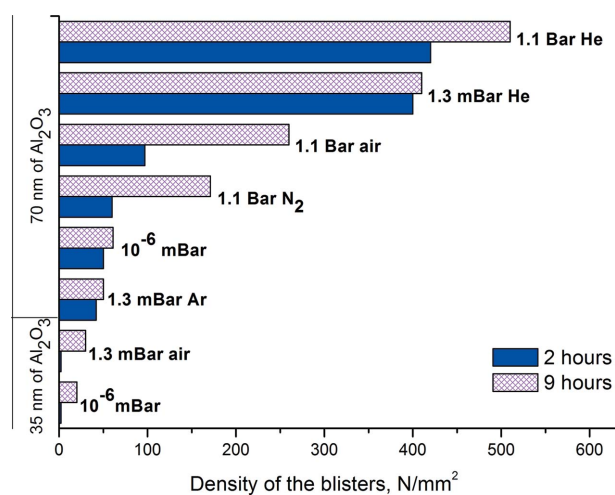


**Figure 5**  
Histogram of the blister density distribution after the white-beam treatment. The thicknesses of the coatings were 35 and 70 nm; exposition times were 2 and 9 h; gaseous conditions are indicated next to the bars.

mechanism of blister formation apart from the release of hydrogen and water due to radiant heating. In our experiments, blister formation was strongly dependent on the type of gas used, so we conclude that the second mechanism of this phenomenon is the penetration of gas molecules into the bulk of the film resulting in the correlation between molecules of the gas used and blister size.

Applied thin film coatings should not only be a barrier against the ambient atmosphere under X-ray illumination but they should also have to possess good mechanical properties in order to provide additional protection for users from hazardous beryllium. The nanoindentation method was used to determine the local physico-mechanical properties (hardness  $H$  and Young's modulus  $E$ ) of the deposited thin film. High mechanical hardness is a key point for the coatings to perform their protection functions.

A typical load/unload  $P(h)$  diagram for studying local deformation processes of the material is shown in Fig. 6. A significant decrease in the indenter penetration depth at equal values of the maximum load  $P_{\max}$  for the sample with coating indicates that nanohardness for the coated sample is higher. Thus, at  $P_{\max} \simeq 0.8$  mN (Fig. 6*b*) the plastic imprint depth for the sample with alumina coating is 35–48 nm, while for the

substrate this value is within the range 55–58 nm. This means that, with the same force applied, the penetration depth for samples with alumina coating is much lower. It should be noted that the deformation of the coatings has a distinct non-monotonic behavior and there are specific shifts (Fig. 6*b*), which could be caused by the nucleation of avalanche dislocations under the indenter during a mode change from elastic to elastic plastic deformation, nucleation and evolution of the cracks, local shear band or phase transitions in the deformation zone (Golovin *et al.*, 2003, 2005; Surmeneva *et al.*, 2015). Deformation of the substrate with the same maximum load either does not experience any shift or their amplitude is significantly lower (Fig. 6).

The study of a size factor effect on the values of local mechanical properties reveals that for all coatings  $H$  and  $E$  increased at the beginning, having a maximum at 20–40 nm imprint depth, and then reduced. They came to a plateau at 80–100 nm imprint depth for samples with aluminium oxide and 140–150 nm for those without coatings.

#### 4. Summary

We examined the performance of aluminium oxide protective coatings applied to beryllium windows under white-beam irradiation in dry air, nitrogen, argon, helium and vacuum atmospheres. Coatings formed by thermal ALD showed their potential applicability in the monochromatic- and pink-beam tests. Enhanced by an alumina layer, the mechanical properties of beryllium provide an additional protection for users. Further research should focus on adjusting the precursor choice to avoid hydrogen incorporation in order to withstand the powerful irradiation of the white beam.

#### Acknowledgements

The authors express their gratitude to the European Synchrotron Radiation Facility (ESRF) in Grenoble for providing the beam time. C. Detlefs and P. Wattecamp are thanked for their invaluable support during the experiments at ID06. The authors also thank A. Borisov, M. Lyubomirsky and P. Ershov for their help in carrying out the experiments with white and monochromatic beams. The authors are deeply indebted to S. Pascarelli for providing the ID24 facility for the pink-beam experiment. S. Medvedeva is acknowledged for performing X-ray reflectometry and diffraction examination of the samples. The work was supported by the Ministry of Education and Science of the Russian Federation. The thermal ALD alumina coating process was developed with the support of the Russian Scientific Foundation.

#### Funding information

The following funding is acknowledged: Ministry of Education and Science of the Russian Federation (award No. 14.Y26.31.0002).

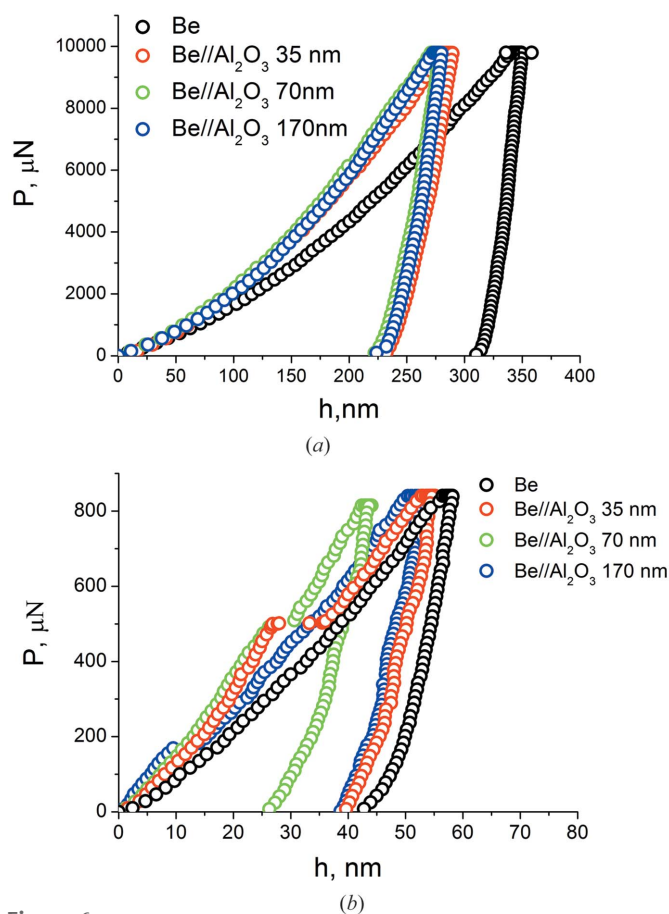


**Figure 6**  
Typical  $P(h)$  diagrams observed during the nanoindentation measurements of beryllium substrate and beryllium substrate coated with ALD alumina of different thicknesses at maximum applied load  $P_{\max} = 10$  mN (a) and  $P_{\max} = 800$   $\mu$ N (b).

References

- Aarik, L., Arroval, T., Rammula, R., Mändar, H., Sammelseg, V., Hudec, B., Hušeková, K., Fröhlich, K. & Aarik, J. (2014). *Thin Solid Films*, **565**, 19–24.
- Beldarrain, O., Duch, M., Zabala, M., Rafí, J. M., González, M. B. & Campabadal, F. (2013). *J. Vac. Sci. Technol. A*, **31**, 01A128.
- Bullock, J., Thomson, A., Cuevas, A., Veith, B., Schmidt, J. & Karkkainen, A. (2013). *Phys. Status Solidi RRL*, **7**, 530–533.
- Elam, J. W., Routkevitch, D., Mardilovich, P. P. & George, S. M. (2003). *Chem. Mater.* **15**, 3507–3517.
- Fedel, M., Zanella, C., Rossi, S. & Deflorian, F. (2014). *Solar Energy*, **101**, 167–175.
- Gmur, N. (1988). *Nucl. Instrum. Methods Phys. Res. A*, **266**, 362–374.
- Gmür, N. (1992). *Nucl. Instrum. Methods Phys. Res. A*, **319**, 228–232.
- Goikhman, A., Lyatun, I., Ershov, P., Snigireva, I., Wojda, P., Gorlevsky, V., Semenov, A., Sheverdyaev, M., Koletskiy, V. & Snigirev, A. (2015). *J. Synchrotron Rad.* **22**, 796–800.
- Golovin, Yu. I., Ivolgin, V. I., Korenkov, V. V. & Tyurin, A. I. (2005). *Phys. Solid State*, **47**, 995–1007.
- Golovin, Yu. I., Ivolgin, V. I., Tyurin, A. I. & Khonik, V. A. (2003). *Phys. Solid State*, **45**, 1267–1271.
- Härkönen, E., Díaz, B., Światowska, J., Maurice, V., Seyeux, A., Vehkamäki, M., Sajavaara, T., Fenker, M., Marcus, P. & Ritala, M. (2011). *J. Electrochem. Soc.* **158**, C369.
- Hecht, E. (2002). *Optics*, 4th ed., edited by A. Black, pp. 506–507. Reading: Addison-Wesley.
- Hennen, L., Granneman, E. H. A. & Kessels, W. M. M. (2012). *Proceedings of the 38th IEEE Photovoltaic Specialists Conference*, Austin, TX, USA, 3–8 June 2012, pp. 001049–001054.
- Knez, M., Nielsch, K. & Niinistö, L. (2007). *Adv. Mater.* **19**, 3425–3438.
- Lyatun, I. I., Goikhman, A. Yu., Ershov, P. A., Snigireva, I. I. & Snigirev, A. A. (2015). *J. Surf. Invest.* **9**, 446–450.
- Oliver, W. C. & Pharr, G. M. (2004). *J. Mater. Res.* **19**, 3–20.
- Snigirev, A., Kohn, V., Snigireva, I. & Lengeler, B. (1996). *Nature (London)*, **384**, 49–51.
- Surmeneva, M. A., Mukhametkaliyev, T. M., Tyurin, A. I., Teresov, A. D., Koval, N. N., Pirozhkova, T. S., Shuvarin, I. A., Shuklinov, A. V., Zhigachev, A. O., Oehr, C. & Surmenev, R. A. (2015). *Surf. Coat. Technol.* **275**, 176–184.
- Tanaka, H., Ishikawa, T., Goto, S., Takano, S., Watanabe, T. & Yabashi, M. (2016). *Proceedings of the Seventh International Particle Accelerator Conference (IPAC'16)*, Busan, Korea, 8–13 May 2016, pp. 2867–2870.
- Winick, H. & Doniach, S. (1980). Editors. *Synchrotron Radiation Research*. New York: Plenum.
- Ylivaara, O., Liu, X., Kilpi, L., Lyytinen, J., Schneider, D., Laitinen, M., Julin, J., Ali, S., Sintonen, S., Berdova, M., Haimi, E., Sajavaara, T., Ronkainen, H., Lipsanen, H., Koskinen, J., Hannula, S.-P. & Puurunen, R. L. (2014). *Thin Solid Films*, **552**, 124–135.
- Yun, S. J., Lee, K.-H., Skarp, J., Kim, H.-R. & Nam, K.-S. (1997). *J. Vac. Sci. Technol. A*, **15**, 2993–2997.
- Yurkevich, O., Maksimova, K., Goikhman, A., Snigireva, I. & Snigirev, A. (2015). *J. Surf. Invest.* **3**, 34–39.